scientific reports

Check for updates

OPEN

In vivo efficacy of NRL knockdown with cell-penetrating siRNA in retinal degeneration

Hyungwoo Lee[1,2,7], Hyoik Jang[3,7], Jae-Byoung Chae[1], Hyo Kyung Lee[4], Chanok Son[1], Chul-Woo Park[1], Taejeong Ha[3], Munjeong Yum[3], Sungmi Park[3], Sun Woo Hong[3], Suk Young Lee[5], Jungmook Lyu[6], Semin Lee[4], Dong Ki Lee[3,5]✉ & Hyewon Chung[1,2]✉

Retinal degenerative diseases, such as retinitis pigmentosa (RP) and age-related macular degeneration (AMD), lead to progressive vision loss through photoreceptor degeneration; RP begins with the gradual loss of peripheral rods, whereas AMD causes central-vision loss mainly because macular cones and parafoveal rods degenerate. The neural retina leucine zipper (NRL) directs rod photoreceptor differentiation, and its disruption has been linked to upregulated cone-specific markers in rods. This study investigates the therapeutic potential of a cell-penetrating asymmetric small interfering RNA targeting NRL (cp-asiNRL) to induce rod-to-cone conversion and mitigate retinal degeneration. cp-asiNRL was administered intravitreally to C57BL/6J wild-type (WT), neovascular AMD (nAMD), and RP ($Rho^{P23H/+}$) mouse models. Subsequent analyses included cone marker expression levels and electroretinographic evaluations, and single-cell RNA sequencing. Administration of cp-asiNRL suppressed NRL expression, increased cone marker expression, and improved retinal function in both WT and nAMD models. In RP mice, cone marker expression was also elevated, although functional improvements were comparatively modest, likely reflecting the advanced disease stage. Single-cell RNA sequencing revealed a rod-to-cone-like transdifferentiation, suggesting that cp-asiNRL-mediated NRL knockdown partially preserved photoreceptor integrity. cp-asiNRL-mediated NRL silencing shows considerable promise as a therapeutic intervention for retinal degenerative conditions. By promoting rod-to-cone transdifferentiation and supporting photoreceptor survival, this approach may offer a novel strategy for vision preservation.

Retinal degenerative diseases are major causes of blindness worldwide. Retinitis pigmentosa (RP) is characterized by the early, progressive loss of peripheral rod photoreceptors, whereas age-related macular degeneration (AMD) primarily compromises macular cones together with parafoveal rods, leading to central vision loss[1–3]. Despite recent advancements, treatment options for these diseases remain limited[4]. For RP, current approaches include artificial retinal prostheses[5]gene therapy, and optogenetic strategies using adeno-associated viruses[6,7]. However, these are still in the early development stages with limited clinical success. Photoreceptor transplantation using precursors derived from pluripotent stem cells has also been explored[8–10], but faces significant challenges such as integration into existing retinal circuitry, functionality of transplanted cells, and safety concerns including teratoma formation[11,12]. For neovascular AMD (nAMD), anti-vascular endothelial growth factor (VEGF) therapies for choroidal neovascularization (CNV) in the fovea are commonly used but may lead to resistance and atrophic degeneration of photoreceptors over time[13,14].

Direct reprogramming, or transdifferentiation, offers a novel strategy for degenerative diseases by converting one differentiated cell type into another without passing through a pluripotent stage[15–17]. This approach has been successfully applied in various tissues; for instance, fibroblasts have been directly converted into cardiomyocytes, neurons, and hepatocytes through the overexpression of specific transcription factors[16,18–20]. In the retina, studies also have shown that Müller glia can be reprogrammed into photoreceptors using transcription factors and small molecules[21,22]. A critical target for such reprogramming efforts is the transcription factor neural retina

[1]Department of Ophthalmology, Konkuk University College of Medicine, Seoul, Republic of Korea. [2]Department of Ophthalmology, Konkuk University Medical Center, 120-1 Neungdong-ro, Gwangjin-gu, Seoul 05030, Republic of Korea. [3]OliX Pharmaceuticals, Inc., Suwon, Republic of Korea. [4]Department of Biomedical Engineering, Ulsan National Institute of Science and Technology, Ulsan, Republic of Korea. [5]Department of Chemistry, Sungkyunkwan University, Suwon, Republic of Korea. [6]Department of Medical Science, Myung-Gok Eye Research Institute, Konyang University, Daejeon, Republic of Korea. [7]Hyungwoo Lee and Hyoik Jang contributed equally to this work. ✉email: dklee@skku.edu; hchung@kuh.ac.kr

leucine zipper (NRL), which plays a key role in rod photoreceptor development by activating nuclear receptor subfamily 2 group E member 3 (NR2E3), thereby suppressing cone-specific genes[23]. Eliminating NRL has been shown to induce rod photoreceptors to adopt cone-like characteristics. As a result, the survival of rod cells is enhanced even in the presence of rod-specific gene mutations, which likely prevents the secondary degeneration of cone cells. Furthermore, in cases of AMD, although cone cells in the macula may be damaged, it is believed that converting the remaining rod photoreceptors into cone-like cells could make them more robust in stressful environments[24]. Genetic deletion of *Nrl* in mice leads to the development of photoreceptors with cone-like properties[25]. Recent studies have utilized gene-editing techniques such as CRISPR/Cas9 to knock out *Nrl* in rod photoreceptors, resulting in improved survival and function of these cells in degenerative models[23]. However, these gene-editing approaches have limitations, including potential immune responses, off-target effects, and challenges with delivery efficiency[26,27].

Small interfering RNA (siRNA) technology has been explored as an alternative to modulate gene expression in retinal cells. Previous studies have used siRNA to target genes involved in retinal neovascularization and degeneration, demonstrating the therapeutic potential of RNA interference in ocular diseases[28,29]. However, traditional siRNA delivery methods often require transfection reagents or viral vectors, which can pose safety risks such as nonspecific retinal toxicity and unwanted immune responses[30–33]. To overcome these challenges, cell-penetrating asymmetric siRNAs (cp-asiRNAs) were introduced. Unlike traditional siRNAs, cp-asiRNAs can efficiently enter cells without the need for transfection agents, significantly reducing potential safety risks[34]. Moreover, cp-asiRNAs have demonstrated superior knockdown efficiency in vivo, and their asymmetric structure helps minimize off-target effects commonly associated with traditional siRNAs[35]. Building upon these advancements, we hypothesized that targeting NRL using cp-asiRNA could facilitate the transdifferentiation of rod photoreceptors into cone-like cells, potentially offering a novel therapeutic strategy for retinal degenerative diseases.

In this study, cp-asiRNA targeting NRL (cp-asiNRL) was developed, and its effect was evaluated in vivo through intravitreal injections. The induced expression of cone-specific genes in rod cells was assessed in mouse models, including the P23H rhodopsin knock-in ($Rho^{P23H/+}$) transgenic mice (an RP model) and a laser-induced CNV model for nAMD. This approach aims to offer a novel and safer therapeutic strategy for retinal degenerative diseases by leveraging the advantages of cp-asiRNA technology for direct reprogramming of photoreceptors.

Methods

Design and synthesis of cp-asiNRL

Sequences targeting NRL were designed for homology with Homo sapiens, Rattus norvegicus, and Mus musculus. Sequence information is provided in Supplementary Table 1. Knockdown efficacies were validated in HeLa cells transfected with the NRL plasmid and in stable NRL-overexpressing A549 cells. Each asiRNA strand was synthesized and purchased from Bioneer (Daejeon, Korea) and transfected using Lipofectamine RNAiMAX (Thermo Fisher Scientific). For knockdown efficiency evaluation in human cell lines, qRT–PCR was performed using specific primers for NRL; forward: 5'-GTCCTGAAGAGGCCATGGAG-3, reverse: 5'-GTTTAGCTCCC GCACAGACA-3'.

After selecting the appropriate asiNRL, cp-asiRNAs were synthesized by Dharmacon™ (Horizon, Colorado, USA). The sense and antisense strands were mixed at a ratio of 1:1 in Opti-MEM (Gibco), heated at 95 °C for 5 min, and cooled at 37 °C for 20 min. The annealing of the cp-asiRNAs was confirmed by electrophoresis on a 12% polyacrylamide gel, followed by staining with EtBr for 10 min.

Cell culture, transfection, and viability assay

HeLa cells (ATCC CCL-2, purchased in March 2017 from the American Type Culture Collection, Manassas, VA, USA) were cultured in DMEM (Invitrogen) supplemented with 10% FBS, 100 U/ml penicillin, and 100 µg/ml streptomycin at 30–50% confluence. After 24 h, cells were transfected with 0.5 µg of NRL plasmid (Origene, RG202237) using Lipofectamine 2000 (Invitrogen) in Opti-MEM™ I Reduced Serum Medium (Gibco). Cells were harvested after 24–48 h for analysis. A549 cells stably expressing NRL were cultured in Ham's F-12 K medium (Gibco) supplemented with 10% FBS and G418 antibiotic (1 mg/ml). Cells were plated in 12-well plates and grown without FBS for 24 h before medium replacement with Opti-MEM containing cp-asiNRL. Cell viability was assessed using an MTT assay kit (Sigma–Aldrich). Cells were seeded in 96-well plates, treated with cp-asiNRL after 24 h, and incubated with MTT reagent. Absorbance was measured at 570 nm.

Experimental animals and procedures for WT and CNV mouse models

All animal experiments were approved by the Konkuk University Institutional Animal Care and Use Committee (IACUC) (KU IACUC; approval no. KU211116). All mice were maintained in accordance with the guidelines of the Konkuk University IACUC and housed under a 12-hour light/12-hour dark cycle at the Konkuk University Laboratory Animal Research Center. All experiments were performed in accordance with ARRIVE guidelines[36]. C57BL/6J male mice were purchased from Orient Bio (Seongnam, Korea) for the WT and CNV mouse model groups. All animal experiments were blinded and randomized. All mice used in the experiments were anesthetized with a combination of Zoletil (Virbac, Carros, France) and xylazine (Bayer, Leverkusen, Germany) at a 4:1 ratio, diluted in normal saline. For experimental analysis, euthanasia was performed by cervical dislocation under deep anesthesia, in accordance with guidelines approved by the Konkuk University IACUC.

At two weeks of age, C57BL/6J mice were subjected to intravitreal injection of cp-asiNRL (0.4 µg/µl) or a control agent—either a non-targeting cp-asiRNA or an equivalent inert compound—and their eyes were collected at five weeks of age. A sterile 30-gauge needle (BD Science, San Jose, USA) was utilized to create a small opening in the limbus, observed under an optical microscope (Olympus SZ51, Tokyo, Japan). Then, a 35-gauge

blunt Hamilton microsyringe (Hamilton Company, NV, USA) was inserted with a 45° injection angle into the vitreous cavity through the hole.

To establish a CNV mouse model, five-week-old mice were anesthetized and the pupils were dilated using single-use topical tropherine eye drops (Hanmi Pharm, Seoul, Korea) containing phenylephrine hydrochloride (5 mg/ml) and tropicamide (5 mg/ml). After anesthesia, laser photocoagulation was performed as described in previous studies to generate a CNV mouse model[37,38]. Three laser spots were created around the optic nerve head in each lubricated eye, which was in contact with a cover slip coated with hypromellose. A slit-lamp laser photocoagulation system (532 nm laser, Carl Zeiss AG, Oberkochen, Germany) was used with the following parameters: 200 mW power, 100 msec duration, and 50 μm spot size. The disruption of Bruch's membrane was confirmed by the generation of bubbles at the photocoagulated site. After the procedures, all eyes were treated with an antibiotic ophthalmic ointment (Tarivid, Santen, Osaka, Japan). Intravitreal injection of cp-asiNRL (0.4 μg/μl) or PBS (as a control) was administered one week after laser treatment. The eyes were then analyzed at eight weeks of age. For analysis, mice were placed in a gas chamber and exposed to CO2 at a constant flow rate of 25% of the chamber volume per minute for 5 min, followed by cervical dislocation. The eyes were then rapidly removed and placed in cold PBS.

$Rho^{P23H/+}$ Transgenic mouse model

Rho$^{P23H/+}$ mice (male and female, one to four months old) were maintained on a C57BL/6J background (Jackson Laboratory)[39]. *Rho*$^{P23H/+}$ transgenic mice were purchased from the Jackson Laboratory (stock no. 000664). The P23H Rho mutation in *Rho*$^{P23H/+}$ transgenic mice leads to the misfolding of rhodopsin in rod photoreceptors. This activates the unfolded protein response, ultimately leading to the death of both rod and cone cells approximately 2 weeks after birth[40]. Therefore, the mice were treated by intravitreal injection of cp-asiNRL (0.4 μg/μl) or PBS as a control on day 14 after birth, and the eyes were subsequently analyzed on day 35. Separate control experiments were performed using a scrambled (non-targeting) cp-asiRNA injected in the same manner, to assess any nonspecific effects of the cp-asiRNA delivery.

Western blot analysis

For cultured cells and mouse retinal tissue, total proteins were extracted with mammalian protein extraction buffer (GE Healthcare, UK) containing a protein inhibitor cocktail (Roche, Switzerland). The protein concentrations were measured using a BCA assay. Equal amounts of protein were separated by SDS–PAGE and transferred to PVDF membranes using the Trans-Blot® SD semidry electrophoretic transfer cell system (Bio-Rad, CA). The membranes were blocked with 5% skim milk for 1 h at room temperature and then incubated with primary antibodies overnight at 4 °C. The following primary antibodies were used: anti-NRL (1:500, Aviva System Biology, OAAB19847), anti-rhodopsin (1:1000, Millipore, MAB5356), anti-Opsin Red/Green (1:1000, Millipore, AB5405), anti-Opsin Blue (1:1000, Millipore, AB5407), and anti-β-actin (1:2500, Santa Cruz Biotechnology, SC-47778). The membranes were washed with Tris-buffered saline containing 1% Tween-20 and incubated for 1 h with secondary antibodies (goat anti-rabbit IgG-HRP: Invitrogen, 31460; goat anti-mouse IgG-HRP: Invitrogen, 31430, 1:10000) at room temperature in 5% skim milk. After incubation, the membranes were treated with enhanced chemiluminescence (ECL) substrate and imaged using a ChemiDoc system (Bio-Rad, CA). The western blot bands were quantified by densitometry using ImageJ software (National Institutes of Health, MD). All experiments were performed at least in triplicate. Full-length blot images are provided in Supplementary Fig. 1 to validate the specificity of the antibodies used.

Immunofluorescence of cryosectioned retinas

The enucleated eye cup was fixed in 4% paraformaldehyde (PFA) for 12 h at 4 °C, transferred to 15% sucrose/PBS, and incubated for 12 h at 4 °C until the tissue sank; subsequently, it was transferred to 30% sucrose/PBS and incubated at 4 °C until the eye cup settled to the bottom of the tube. Then, the eyecup was embedded in OCT compound (FSC 22 Clear Frozen Section Compound; Biosystems Inc., Wetzlar, Germany) and subsequently sectioned (Leica CM1860, Leica Biosystems Inc.) at a thickness of 10 μm.

Tissues were fixed with 4% PFA for 20 min at room temperature and permeabilized with 0.1% Triton X-100 in PBS for 15 min. After blocking with 5% BSA in PBS for 1 h, fixed tissues were incubated overnight at 4 °C with primary antibodies against Anti-Opsin antibody, blue (1:1000, Sigma-Aldrich, AB5407, MO, USA), Anti-Opsin antibody, Red/Green (1:1000, Sigma-Aldrich, AB5405), Anti-Rhodopsin antibody (1:2000, Millipore, MAB5356), Anti-Cone-Arrestin (1:1000, Sigma-Aldrich, AB15282) or Anti-Cngb3 (1:200, Santa Cruz Biotechnology, sc-398211). The stained tissues were washed with PBS for 5 min twice and incubated for 2 h at room temperature with the following Alexa Fluor-conjugated secondary antibodies: Alexa Fluor 555-conjugated goat anti-rabbit IgG (Thermo Fisher Scientific, A-21424), or Alexa Fluor 488-conjugated goat anti-rabbit IgG (Thermo Fisher Scientific, A-11034). All secondary antibodies were used at a dilution of 1:1000. After incubation with secondary antibodies, tissues or cells were stained with the nuclear dye Hoechst 33,342 (1:3000, Thermo Fisher Scientific, H3570) in PBS for 15 min at room temperature. Afterward, tissues were mounted with mounting medium (Polysciences, 18606–20, PA, USA). The stained cells at dorsal retina were observed with an inverted microscope (LSM900, Oberkochen, Germany).

TUNEL apoptosis assay

To detect cell apoptosis, sectioned retinal tissues were fixed in 4% PFA for 15 min and stained using an in situ cell death detection kit, fluorescein (Roche, 11684795910), for 1 h 30 min in a 37 °C incubator following the manufacturer's instructions, and nuclei were counterstained with Hoechst 33,342. Images were obtained using a fluorescence microscope with an AxioCam camera (Zeiss) or a confocal microscope (LSM510 PASCAL, Zeiss).

To quantify the number of TUNEL-positive cells stained with Hoechst 33,342, at least 6 retinal tissues were observed at a 63× magnification.

Full-field electroretinogram

Dark-adapted (scotopic) and light-adapted (photopic) full-field electroretinograms (ERGs) were recorded to assess overall retinal function and visual impairments, utilizing the Celeris rodent electrophysiology system (Diagnosys LLC, Lowell, MA, USA). Mice underwent dark adaptation for over 12 h prior to the scotopic experiments and were prepared for ERG recordings under deep red illumination. Following pupil dilation with topical tropherine eye drops (Hanmi, Korea), the mice were anesthetized with a mixture of Zoletil (Virbac, France) and xylazine (Rompun, Bayer HealthCare, Germany), then placed on a heated stand to facilitate the measurement of ERG signals. The eyes were lubricated with 2% hypromellose, and the corneal electrode was positioned accordingly. The scotopic test was conducted using pulsed white light at gradually increasing intensity. After 5 min of light adaptation, photopic ERGs were recorded with brighter white flashes at escalating stimulation intensities. Post-ERG measurements, the ointment was applied to both eyes, and the mice were returned to the animal room once they had fully recovered on a warm heating mat.

scRNA-seq data generation and analysis

The retinal cells were gently resuspended after being washed twice at 4 °C for 5 min at 300 g in cold Ca2+- and Mg2+-free 0.04% BSA/PBS. Cells were counted with a LUNA-FX7™ Automated Fluorescence Cell Counter (Logos Biosystems) with acridine orange (AO) and propidium iodide (PI) staining (Logos Biosystems, cat no. F23001).

A 10x Chromium controller and Next Gem Single Cell 3' Reagent v3.1 kits (10x Genomics, PN-1000123) were used to prepare single-cell RNA-seq libraries according to the 10x Chromium Single Cell 3' v3.1 protocol (10x Genomics, document no. CG000315). To generate a single-cell gel bead-in-emulsion (GEM), the cell suspension (10,000 cells recovered from the target) was mixed with reverse transcription master mix and loaded with single-cell 3′ gel beads and partitioning oil into a single-cell G chip (10x Genomics, PN-1000120). Poly-adenylated mRNA from single cells was uniquely barcoded and reverse-transcribed within GEM. After barcoded full-length cDNA was generated from mRNA through GEM-RT incubation, the barcoded cDNA molecules were amplified via PCR. For 3' gene expression library construction, the enriched cDNA was sequentially subjected to enzymatic fragmentation, end repair, A-tailing, adaptor ligation and index PCR.

Following the qPCR Quantification Protocol Guide (KAPA), the purified libraries were quantified using qPCR and validated using the Agilent Technologies 4200 TapeStation (Agilent Technologies). The sequencing was performed on the Illumina NovaSeq platform.

FASTQ files were mapped to the mouse reference genome (mm10). Quality control and gene expression matrices were generated using the Cell Ranger pipeline (version 7.0.1). Data analysis was performed with the Seurat package (version 4.3.0). Cells with fewer than 200 unique genes, more than 1,000 genes, or over 10% mitochondrial reads were filtered out, resulting in 21,959 genes across 19,047 cells.

Cells were divided into 31 clusters based on the top 15 principal components using FindClusters with a resolution parameter of 0.6. The marker genes *Pde6a*, *Ppef2*, *Nr2e3*, *Gnat2*, *Opn1mw*, *and Opn1sw*[41] in photoreceptor cells (rod and cone) were activated in 1, 21, 29 of the 31 clusters. FindClusters was used to divide the cells of photoreceptor subclusters into clusters based on the top 10 principal components, with the resolution parameter set to 0.4. Uniform manifold approximation and projection (UMAP) was used for visualization. To compare cp-asiNRL and PBS samples, we defined the dashed-line significance threshold by a $\log_2$(fold change) of ≥ 0.5 and an adjusted p-value of ≤ 0.05, ensuring that only genes meeting these criteria were labeled as significantly altered.

Trajectory analysis was conducted by Monocle2 (version 2.22.0). Pseudotime was computed using Monocle2, to represent the biological progression of reconstructed differentiation trajectories or inferred cellular states based on specific genes. Cells with an expression level greater than 0.1 (min_expr = 0.1) were identified and genes with more than 0 in the total expression of all cells were used. The genes used in trajectory analysis were selected based on the photoreceptor subclusters using FindAllMarkers (min.pct = 0.25, logfc.threshold = 0.25, test.use="wilcox", assay="RNA", slot="data"). Dimensional reduction was implemented using reduceDimension (max_components = 4, method='DDRTree', norm_method='log'). Then, the results were visualized by the plot_cell_trajectory function in Monocle2.

Gene expression comparisons were performed using the Kruskal – Wallis test. All packages used in the analysis were implemented in R (version 4.1.1).

Statistics

The data are presented as the means ± standard deviations of at least three independent measurements. Statistical significance (P values) was assessed using unpaired two-tailed Student's t tests for comparisons between two groups, while multiple datasets were analyzed through one-way ANOVA, followed by Tukey's multiple comparisons test. All statistical analyses were conducted using GraphPad Prism 5 software (San Diego, CA, USA). The criteria for determining statistical significance were as follows: *, $P < 0.05$; **, $P < 0.01$; and ***, $P < 0.001$.

Results

Design and selection of cp-asiNRL

The NRL-targeting siRNA was designed using the asymmetric form of the 16-mer (sense strand) and 25-mer (antisense strand) considering the homology of the *Homo sapiens* (H), *Rattus norvegicus* (R), and *Mus musculus* (M) sequences. A total of 73 distinct sequences were designed that were 100% identical to human

NRL, including one or two nucleotide mismatches between rat/mouse and human, respectively (Supplementary Fig. 2A). Additionally, the overall asiNRL sequences were narrowed to the final 40 sequences targeting 4 identified human *NRL* transcript variants. To validate the designed asiNRL, a plasmid carrying the human NRL gene was transfected into HeLa cells, which were then treated with 40 asiNRL (3 nM) after 24 hours. Although up to 10 nM achieved near-complete knockdown (data not shown), 3 nM was selected to stay within the dose-response range, enabling clear comparison of knockdown efficiencies among asiRNA constructs. Seven asiNRLs (#47, #48, #49, #67, #68, #72, and #73) decreased NRL mRNA expression by more than 40% (Supplementary Fig. 2B). To confirm the knockdown efficacy at the protein level, the selected 7 asiNRLs (3 nM) were transfected into cells and harvested 48 h after transfection, followed by western blotting analysis. Compared with the plasmid alone (Mock), four asiNRLs (#47, #49, #67, and #68) reduced NRL protein expression by more than 70% (Supplementary Fig. 2C). The half-maximal inhibitory concentration (IC50) of asiNRL #47 was determined to be 108.9 pM based on the NRL protein expression level ($R^2 = 0.992$), in addition to the other 3 sequences (Fig. 1A and Supplementary Fig. 2D).

To protect the naked siRNA from exonucleases and endonucleases, the phosphate backbone at the 3' end of the sense and antisense strands was substituted with phosphorothioate, and the 2' OH of the sugar was substituted with -O-methyl or -fluoro modifications. The cholesterol/lipophilic moiety was conjugated to the 3' end of the sense strand to increase cellular uptake[42,43]. These chemical modifications were introduced into the selected asiNRL #47 to increase the penetration of cell membranes without any delivery reagents (Fig. 1B). To assess the effects of this cp-asiNRL, a cell line stably overexpressing the human NRL gene (A549/NRL cell line;

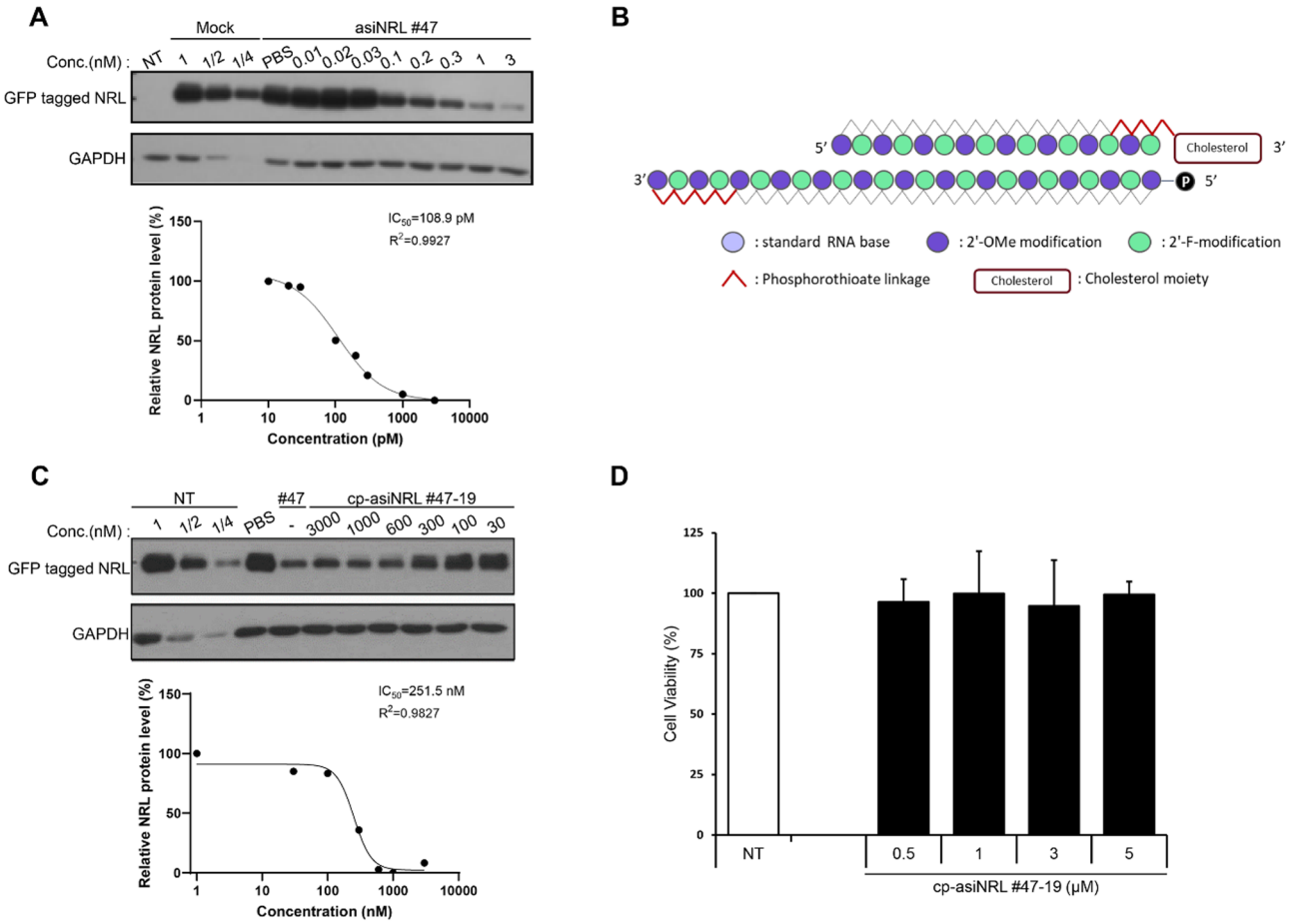

Fig. 1. Molecular design and selection of cell-penetrating asymmetric small interfering RNA targeting NRL (cp-asiNRL). (A) Half-maximal inhibitory concentration (IC50) of the potent asiNRL #47. HeLa cells overexpressing human NRL were incubated with various concentrations ranging from 0.01 to 3 nM asiNRL #47 after transfection for 48 hours, followed by western blotting analysis, and the bands were normalized to those of GAPDH. (B) To confer cell-penetrating ability to asiRNAs, chemical modifications were introduced into the sugar-phosphate backbone, and a cholesterol moiety was conjugated at the 3' end of the sense strand. (C) IC50 of the comparative cp-asiNRL #47 – 19. The A549 cell line constitutively overexpressing GFP-tagged NRL (A549/NRL) was incubated in the range of 30 to 3000 nM for 72 h by passive uptake, followed by western blotting analysis, and the bands were normalized to those of GAPDH. (D) Cell viability of cells treated with cp-asiNRL #47 – 19. The cells were incubated for 24 h with various concentrations of cp-asiNRL #47 – 19 (0.5, 1, 3, and 5 μM), followed by the MTT assay. The data are shown as the mean ± SD of 3 independent experiments. NT; non-treated.

data not shown) was developed. For the first chemical modification, three sense and three antisense strands were designed following the differentiation strategy based on the number and position of the 2'-O-methyl and 2'-fluoro modifications. In three independent experiments, cp-asiNRL #47 labeled with 2 S:2AS (1 μM) most efficiently decreased the expression of the target NRL mRNA gene (Supplementary Fig. 3A and B).

The second chemical modification included the substitution of the phosphate backbone at the 5' end of both strands with phosphorothioate and the addition of a phosphate group at the 5' end of the antisense strand. The phosphate group at the 5' end is essential for guiding strands in siRNA duplexes for loading into *Ago2*.[35,44] Therefore, 2S-1, 2AS-1, and 2AS-2 were synthesized with different modification patterns. Among the five different modification patterns, cp-asiNRL #47 2S:2AS-1 (named #47 – 19) most efficiently decreased NRL protein expression (Supplementary Fig. 3C and D). Next, the IC50 of cp-asiNRL #47 – 19 on NRL protein expression in A549/NRL cells was determined. cp-asiNRL #47 – 19 appeared to reduce the expression of NRL by 50% at 300 nM (IC50 = 251.5 pM, $R^2 = 0.9827$) (Fig. 1C).

Finally, MTT assays were performed to investigate whether cp-asiNRL #47 – 19 could affect cell viability. The assays were conducted 24 h after treatment with cp-asiNRL #47 – 19 at various concentrations. Cell viability did not change between 0.5 to 5 μM cp-asiNRL #47 – 19 (Fig. 1D). These findings suggest that lower concentrations, including the 300 nM used to determine the IC_{50}, are likely non-toxic. Therefore, we ultimately selected cp-asiNRL #47 – 19, which could be effectively delivered into ocular tissues and effectively reduce the expression of NRL.

In the $Rho^{P23H/+}$ transgenic mouse model of RP, we intravitreally injected scrambled siRNA or cp-asiNRL. While scrambled siRNA treatment did not alter NRL protein levels compared to those in WT mice, administering cp-asiNRL led to a decrease in NRL protein in retinal tissue, while the statistical significance was not fulfilled (Supplementary Fig. 4). These results confirm the in vivo efficacy of our cp-asiNRL treatment.

Efficacy of cp-asiNRL in the WT mouse model

To assess the in vivo knockdown efficacy of cp-asiNRL, C57BL/6J wild-type mice received intravitreal injections of cp-asiNRL. Retinas were subsequently isolated and analyzed for photoreceptor gene expression. As expected, cp-asiNRL treatment reduced NRL expression. In addition, the levels of cone markers (OPN1SW, OPN1MW) were elevated following cp-asiNRL treatment (Fig. 2A and B). Immunofluorescence images of PBS- and cp-asiNRL-treated retinas showed that OPN1SW- and OPN1MW-positive rods were more abundant in cp-asiNRL-treated mice than in control mice (Fig. 2C and D).

In ERG, under scotopic conditions, cp-asiNRL did not alter rod-driven b-wave amplitudes at any intensity (Fig. 2E). A modest but significant increase in the scotopic a-wave was observed only at flash intensities ≥ 1 cd·s/m^{-2}, a luminance at which the response is dominated by cones after rod saturation. By contrast, photopic a- and b-wave amplitudes were significantly elevated across the tested range (≥ 10 cd·s/m^{-2}) in cp-asiNRL-treated eyes, indicating a selective enhancement of cone-mediated function while rod responses remained stable in WT retina.

Efficacy of cp-asiNRL in a CNV mouse model and the rescue of retinal degeneration

Because the primary cause of central vision loss in nAMD patients is the loss of foveal cone cells, despite extensive treatments, we evaluated the effectiveness of cp-asiNRL in a CNV mouse model. In this model, cp-asiNRL treatment significantly reduced the expression of NRL and decreased the rod marker (Fig. 3A and B). Additionally, cone opsin expression (L/M-opsin) was statistically higher in cp-asiNRL–treated eyes than in control eyes in this model (Fig. 3B), consistent with a partial shift toward a cone photoreceptor phenotype. ERG analysis showed a recovery of scotopic a- and b-wave amplitudes after cp-asiNRL treatment. By contrast, photopic a- and b-waves did not differ significantly from controls (Fig. 3C), indicating that cone-mediated functional rescue was not detectable under the current dosing and study window (Fig. 3C).

Efficacy of the cp-asiNRL in an RP mouse model and the rescue of retinal degeneration

Next, we evaluated the effect of cp-asiNRL in an RP mouse model using $Rho^{P23H/+}$ transgenic mice. Compared with control eyes, cp-asiNRL treatment reduced the expression of rhodopsin (RHO) and increased the expression of cone markers, particularly OPN1MW (L/M-opsin), suggesting transdifferentiation from rods to cones (Fig. 4A and B).

Immunofluorescence images of control and cp-asiNRL-treated retinas showed that S-opsin- and L/M-opsin-positive rods were more abundant in cp-asiNRL-treated mice (Fig. 4C and D). Furthermore, eyes treated with a non-targeting scrambled cp-asiRNA (Scramble control) showed no significant changes in cone-markers Arrestin and S-opsin (Supplementary Fig. 5). By contrast, cp-asiNRL-treated eyes exhibited markedly higher cone marker expression than did Scramble-treated eyes (Supplementary Fig. 5). To further distinguish newly reprogrammed photoreceptors from pre-existing cones, we conducted co-staining with two independent cone markers, S-opsin and Cngb3, on adjacent retinal sections (Supplementary Fig. 6). cp-asiNRL treatment significantly increased the expression of both markers individually, but the area of overlap between the two markers did not increase significantly, suggesting that the induced cone-marker-positive cells were predominantly distinct from native cones. TUNEL assays showed that photoreceptor apoptosis in $Rho^{P23H/+}$ mice was decreased by intravitreal injection of cp-asiNRL (Fig. 4E).

In ERG, partial recovery of the b-wave under scotopic conditions and partial recovery of both the a- and b-waves under photopic conditions were observed (Fig. 4F). Nevertheless, none of these ERG changes in the $Rho^{P23H/+}$ model reached statistical significance. Taken together, our findings indicate that cp-asiNRL can up-regulate cone-specific genes and induce a cone-like phenotype in degenerating photoreceptors—an encouraging molecular effect that merits further investigation, even though robust functional rescue has yet to be demonstrated.

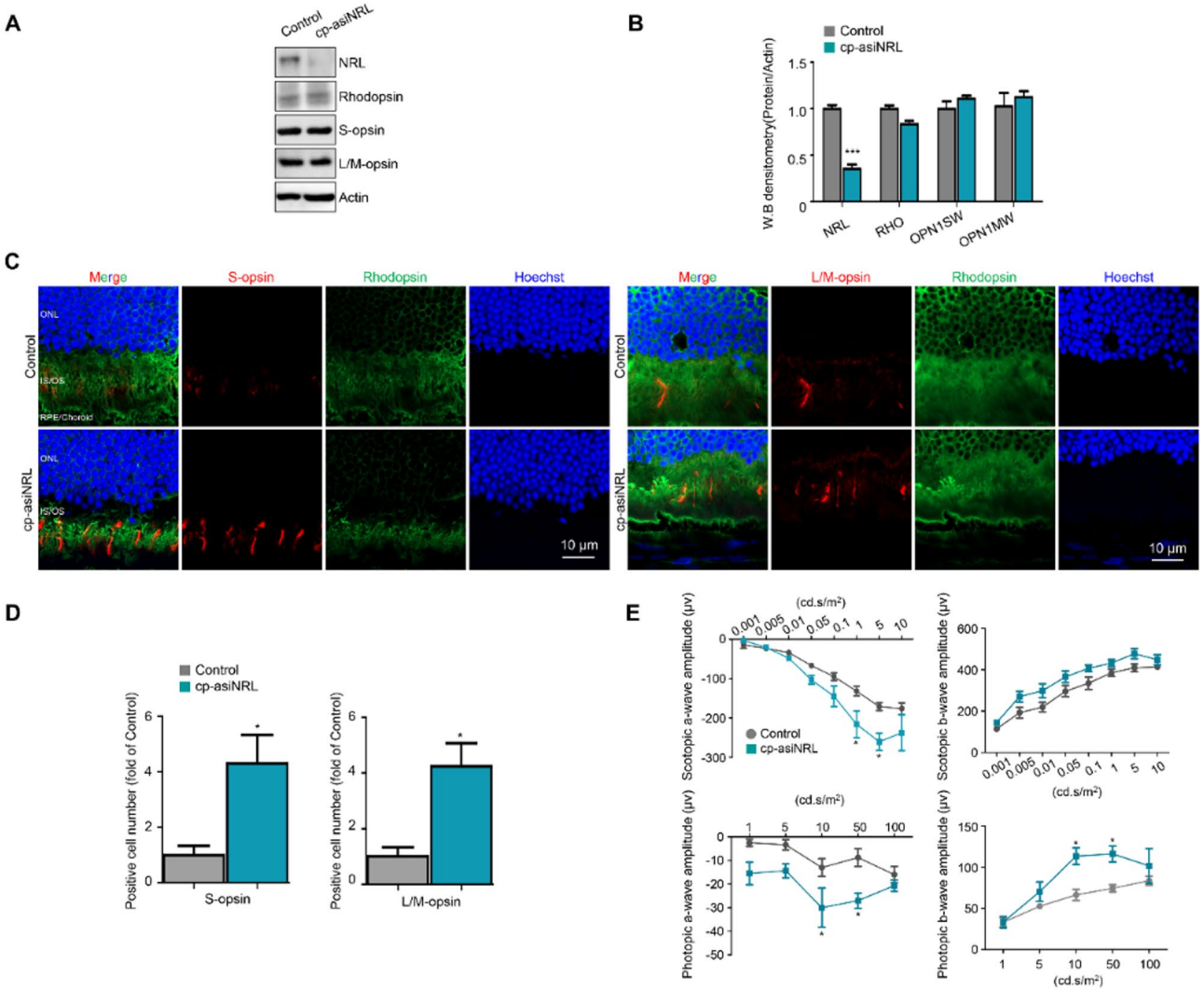

Fig. 2. cp-asiNRL knockdown efficacy in WT mice. (A) Representative western blot images. (B) Relative densitometric bar graphs ($n = 4$ per group). (C) Immunohistochemistry images dorsal retinal sections showing cone and rod markers in WT mice. (D) Quantification of the number of cells displaying positive fluorescence for S-opsin and L/M-opsin in control and cp-asiNRL-treated retinas. Data are presented as mean ± SD ($n = 3$ per group). (E) Electroretinogram under scotopic and photopic conditions. Note that the scotopic a-wave shows significance only at intensities ≥ 1 cd·s/m^{-2}, reflecting cone contribution after rod saturation. ($n = 4$ per group). *$p < 0.05$.

scRNA-seq data analysis

To assess the biological changes of *Nrl* knockdown in the photoreceptor-degenerative retina at the single-cell level, two groups were generated from the RP mouse model using *Rho*$^{P23H/+}$ transgenic mice: cp-asiNRL, a case RP model in which the expression of the *Nrl* gene is disrupted using cp-asiNRL, and PBS, a control RP model. Using 10x Genomics Chromium, 19,047 retinal cells were identified after filtering low-quality cells (Fig. 5A and Methods section). Based on the expression of cell type-specific marker genes[41,45–47], we detected thirteen different retinal cell types (Fig. 5B and C).

To investigate the transcriptomic changes resulting from *Nrl* knockdown in degenerative photoreceptor cells, 2,044 rod and cone photoreceptor cells were separated according to the expression of marker genes[41]. According to unsupervised classification, the photoreceptor clusters were divided into 6 subclusters. The rod photoreceptor cluster with high expression of rod marker genes was located in clusters 0, 1, and 3. In contrast, the cone photoreceptor cluster with high expression values of cone marker genes was distributed in clusters 2 and 4 (Fig. 5D). Comparison of the cp-asiNRL and PBS groups revealed that cone photoreceptor marker genes were significantly upregulated in the cp-asiNRL group compared to PBS, whereas rod-specific markers showed little change (Fig. 5E). This differential expression pattern strongly supports the conclusion that cp-asiNRL drives photoreceptors away from a rod identity toward a conelike phenotype in the RP mouse model.

To verify the transcriptomic dynamics in photoreceptor cells caused by *Nrl* knockdown in the RP model, trajectory analysis was performed. Two main branches were identified, and the direction of the pseudotime was

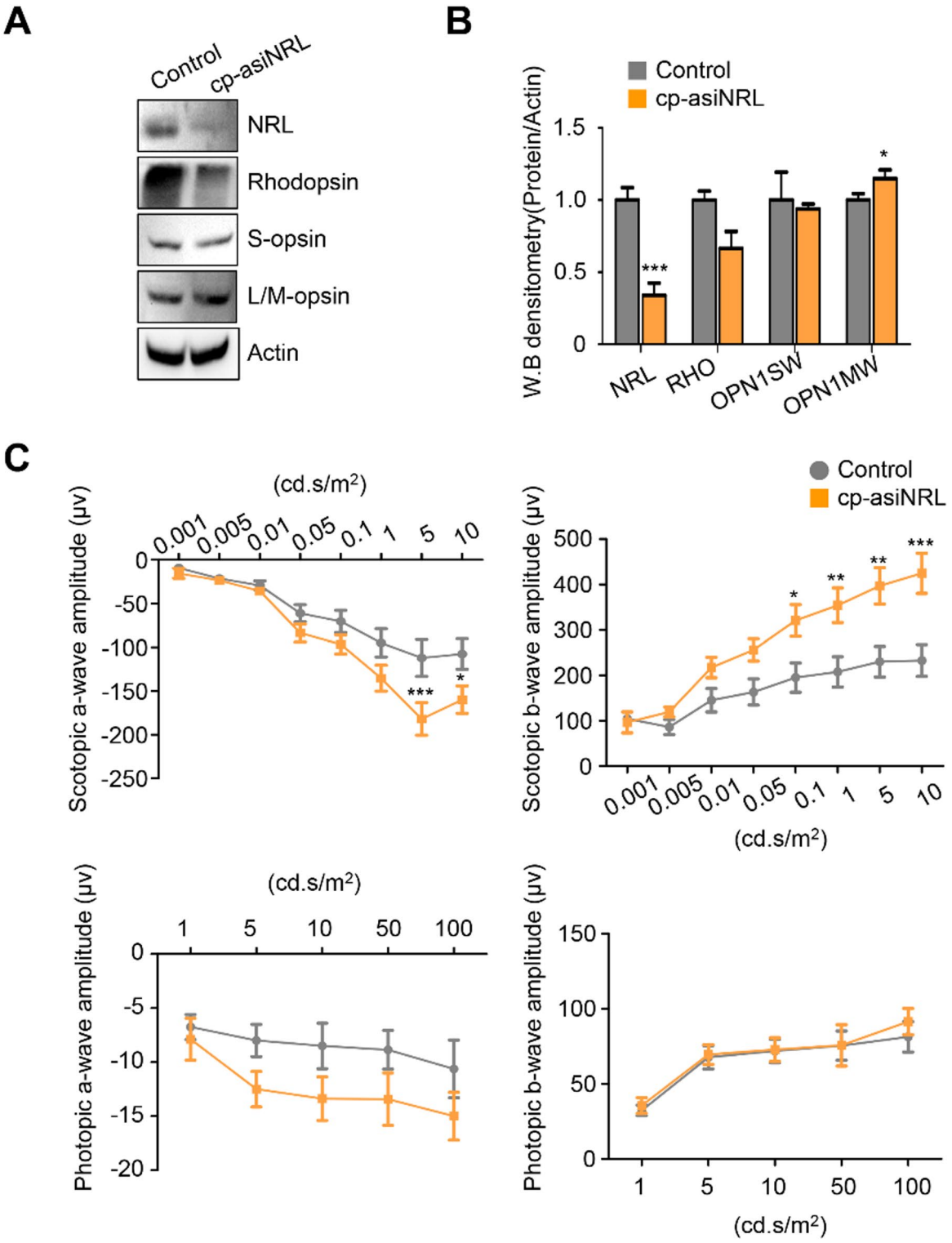

Fig. 3. Cp-asiNRL knockdown efficacy in the CNV mouse model. (A) Representative western blot images. (B) Relative densitometric bar graphs ($n = 3$ per group). (C) Electroretinogram under scotopic and photopic conditions ($n = 7$ per group). *$p < 0.05$.

left to right. The rod photoreceptor clusters were located mainly on the left side of the pseudotime branches. On the right side, cone photoreceptor clusters were distributed. Cluster 2, a cone photoreceptor cluster, was predominant at the end of the pseudotime analysis. At the midpoint of pseudotime, cluster 4 was the key hub of the transcriptomic dynamics transition from rods to cones (Fig. 5F). Furthermore, the expression of *Nrl* was the lowest in cluster 2, and the second lowest cluster was cluster 4 (Fig. 5G). In addition, the ratio of cp-asiNRL-

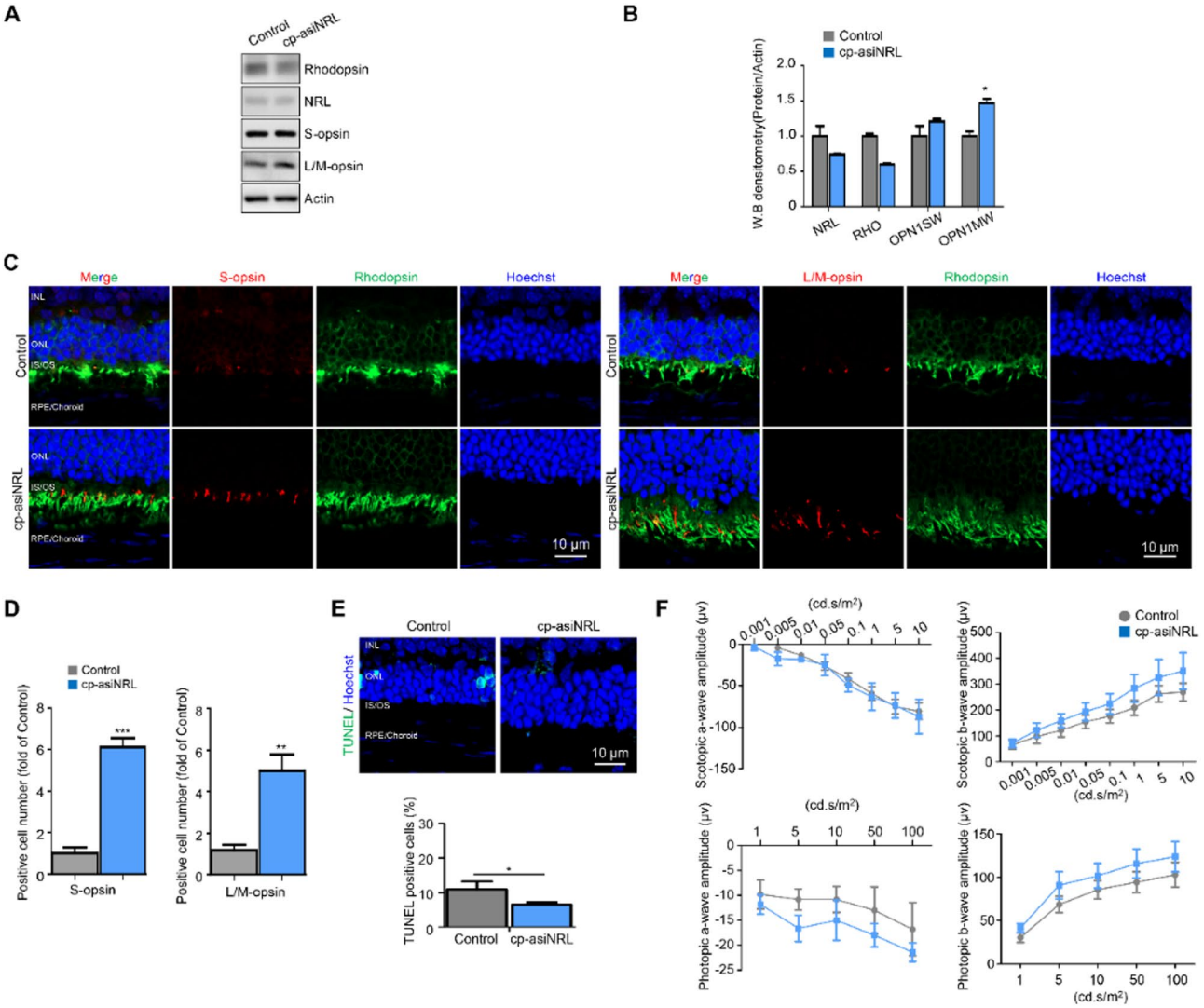

Fig. 4. cp-asiNRL knockdown efficacy in Rho$^{P23H/+}$ transgenic mice. (A) Representative western blot images. (B) Relative densitometric bar graphs ($n = 4$ per group). (C) Immunohistochemistry images showing cone- and rod-specific markers in the dorsal retina. (D) Quantification of the number of cells displaying positive fluorescence for S-opsin and L/M-opsin in control and cp-asiNRL-treated retinas. Data are presented as mean ± SD ($n = 3$ per group). (E) Representative images of apoptosis in the outer retinal layer were detected using a TUNEL assay. The blue color denotes all nuclei, and the green color denotes DNA-damaged nuclei. The graph shows a significantly decreased ratio of apoptotic nuclei in the cp-asiNRL-treated group compared to the control group. (F) Electroretinogram under scotopic and photopic conditions ($n = 5$ per group). *$p < 0.05$.

treated cells to PBS-treated cells in each cluster increased from rod clusters (#3-0-1-5) to cone clusters (#4 – 2) (Fig. 5H). As a result, cluster 4 was estimated to be composed of cone-like cells. When comparing three types of cells, rod, cone-like, and cone, the expression of rod marker genes decreased, and the expression of cone marker genes increased in the order of rod, cone-like, and then cone (Fig. 5I). In conclusion, these results suggest that *Nrl* knockdown can restore retinal function by changing the characteristics of degenerating photoreceptor cells from rods to cone-like photoreceptors.

Discussion

In this study, cp-asiNRL was applied to mouse models of degenerative retinal diseases, including RP and its potential therapeutic benefit was demonstrated. To our knowledge, this is the first report of siRNA-mediated transdifferentiation of postmitotic photoreceptors in vivo. Previously, Yu et al. demonstrated in *Nrl*-knockout models that rod photoreceptors can acquire cone-like morphological features[25]. In their study, toluidine blue-stained semi-thin sections and electron microscopy revealed that, in contrast to control retinas (which had small, heterochromatin-rich rod nuclei), the *Nrl* knockout retinas contained some photoreceptors with cone-like nuclei (larger size with a greater euchromatin content). Additionally, AAV-CRISPR/Cas9-transduced rods exhibited reduced expression of several rod-specific genes and enhanced expression of cone-specific genes[25].

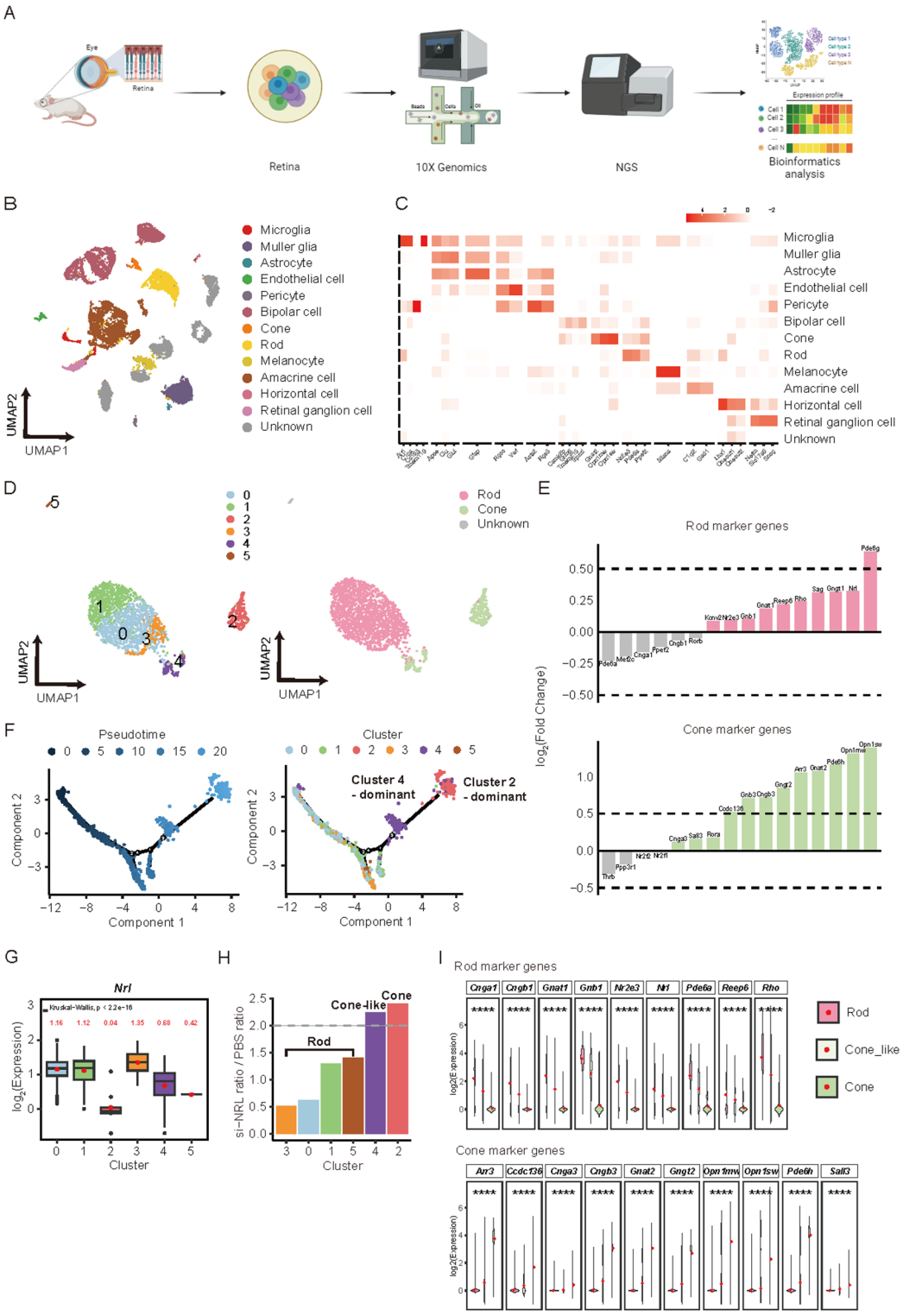

Fig. 5. scRNA-seq data analysis. (A) Workflow of the scRNA-seq analysis. (B) UMAP of 13 cell types detected in retinal cells. (C) Heatmap of marker gene expression values in 13 cell types. (D) UMAP of photoreceptor cells. (E) Bar plots of $\log_2$(fold change) of marker genes in rod and cone photoreceptors; the black dashed line indicates a $\log_2$(fold change) of 0.5, the significance threshold, compared to the cp-asiNRL and PBS groups. (F) Trajectory analysis of photoreceptor cells using Monocle2. (G) The expression levels of the *Nrl* gene in 6 subclusters. (H) The ratio of the cp-asiNRL ratio to the PBS ratio to the cell count in 6 clusters; the gray the dashed line denotes the 2-fold significance cutoff. (I) Violin plot of marker genes in three types of cells, namely, rod, cone-like, and cone cells.

They showed that the rod cells gained partial features of cones, and as a result, their survival in *Rho*$^{-/-}$, *Rd10*, and *Rho-P347S* mice improved. Inspired by that proof-of-concept, we utilized cp-asiNRL to knock down *Nrl* in adult mice, achieving comparable rod-to-cone gene expression changes in both a rod-dominant RP model and a CNV-induced retinal degeneration model. cp-asiRNAs are asiRNAs with a shortened passenger strand (16 nucleotides) and show reduced nonspecific effects compared with conventional siRNAs. cp-asiRNAs have chemical modifications, including phosphorothioate, nucleic acid, and 2'-O-methyl and fluoro modifications, which increase endocytosis, enhance interactions with the cell membrane and uptake, increase the stability of siRNA and reduce immune reactions[35,48–51]. Given these characteristics, it was hypothesized that cp-asiNRL might be more useful for clinical application than the CRISPR/Cas9 system, the in vivo use of which faces two significant challenges—unwanted immune responses induced by the expression of the bacterial protein Cas9 and off-target editing[26,27].

In wild-type mice, partial knock-down of *Nrl* by cp-asiNRL elevated cone-specific markers in the outer retina (Fig. 2D). Functionally, cp-asiNRL selectively increased cone-mediated electroretinographic responses (Fig. 2E): photopic a- and b-wave amplitudes increased significantly at all luminances, whereas scotopic b-waves remained unchanged. A modest rise in the scotopic a-wave was evident only at flash intensities ≥ 1 cd·s/m^{-2}, a range dominated by cone activity after rod saturation. Collectively, these findings suggest that cp-asiNRL steers a subset of rods toward an intermediate cone-like state, enhancing cone output without compromising baseline rod function.

We further validated the effect of cp-asiNRL in a laser-induced CNV mouse model. In nAMD, CNV mainly develops at the macula, damaging both foveal cone cells and parafoveal rod cells. However, some rod cells at the parafovea and perifovea remain, depending on the extent of the disease. Transdifferentiation of the remaining parafoveal rod cells into cone-like cells can improve central vision. Additionally, the standard-of-care treatment (anti-VEGF therapy) can be combined with cp-asiNRL to achieve better visual acuity than can anti-VEGF therapy alone because their mechanisms of action are different. In the CNV model, we observed no statistically significant improvement in full-field photopic ERG, likely because focal RPE disruption and outer-segment loss dampen cone signals and mask modest gains from partial rod-to-cone conversion; longer treatment windows or larger cohorts will be required to reveal any cone-mediated benefit.

Finally, the *Rho*$^{P23H/+}$ mouse model responded favorably to cp-asiNRL treatment produced a trend toward improved ERG responses relative to controls, though not statistically significant, indicating partial preservation of function. cp-asiNRL increased the protein levels of cone-specific markers, indicating a transdifferentiation effect on the rods. Consistent with rod-to-cone reprogramming, cp-asiNRL–treated retinas showed reduced rhodopsin and markedly increased cone-specific proteins by Western blot and immunofluorescence compared to controls. This result was also supported by trajectory analysis from the scRNA-seq experiment, which revealed a transcriptomic transition from rods to cone-like cells following cp-asiNRL treatment in the retina of Rho$^{P23H/+}$ mice, suggesting that *Nrl* knockdown restored retinal function by promoting the conversion of rods into cone-like photoreceptors. To determine whether this increase reflected expansion of native cones or conversion of rods, we performed dual immunostaining for two independent cone markers (Sopsin and Cngb3). cpasiNRL treatment enlarged the territory of each marker individually, whereas the fractional overlap between the two did not change significantly compared with scrambled controls, indicating that most of the additional conemarkerpositive cells are newly reprogrammed photoreceptors rather than preexisting cones (Supplementary Fig. 6). Complementing these protein level findings, pseudotime trajectory analysis from scRNA-seq data revealed a transcriptomic shift from rod cells to cone-like cells in the retina of cp-asiNRL-treated *Rho*$^{P23H/+}$ mice. Together with earlier reports that rods can survive in the absence of NRL expression in both patients and animal models[52,53], these results support the conclusion that partial *Nrl* knockdown remodels degenerating rods into conelike photoreceptors and thereby offers a mechanistically distinct avenue to sustain retinal function. Unlike the acute, tamoxifen-induced Nrl knockout reported by Montana et al., which produced a pronounced loss of scotopic a- and b-wave amplitudes[24], our cp-asiNRL treatment achieves only partial *Nrl* suppression and preserves rod function. This discrepancy may stem from the degree of NRL suppression, timing and delivery methods (gradual siRNA-mediated knockdown vs. an abrupt, tamoxifen-driven Cre system), and experimental variables such as mouse strains or ERG protocols. Additionally, future studies should evaluate cp-asiNRL in other relevant models of altered photoreceptor fate. For example, the Nr2e3$^{rd7/rd7}$ mouse (a model of enhanced S-cone syndrome caused by Nrl dysfunction) could provide further insight into the effects of *Nrl* knockdown on rod-to-cone reprogramming[54].

Our study has several limitations. First, although we tested three commercially available antibodies, a proper antibody for immunofluorescence staining to detect NRL was unavailable. Therefore, immunofluorescence assessment of rhodopsin and S-opsin was used to indirectly demonstrate the effectiveness of cp-asiNRL. Second, we did not directly confirm the penetration and localization of cp-asiNRL into the photoreceptor layer in vivo; future studies should include experiments to verify cp-asiNRL localization in retinal tissues. Third, in the *Rho*$^{P23H/+}$ mouse model, the knockdown of NRL did not reach statistical significance, which may have limited the observed therapeutic effects; optimizing cp-asiNRL variants with improved knockdown efficiency could enhance outcomes in future studies. Fourth, in contrast to the more pronounced functional deficits reported by Yu et al.[25] and Montana et al.[24]our data indicate that cp-asiNRL treatment induces rod-to-cone transdifferentiation; however, the improvement in retinal function measured by ERG is relatively modest. This modest functional gain may be attributable to an incomplete knockdown of *Nrl*, a limited extent of transdifferentiation, or variations in the delivery efficiency of cp-asiNRL compared to viral vector approaches. Finally, we did not perform electron microscopy (TEM), which would offer more definitive morphological evidence of rod-to-cone conversion, as demonstrated by Yu et al.[25]. We plan to include TEM in future studies to confirm ultrastructural changes. Instead, our conclusions are supported by comprehensive transcriptomic and immunohistochemical analyses, and we plan to incorporate TEM in future investigations to further validate these findings.

In conclusion, our study provides the first evidence that intravitreal treatment with cp-asiNRL could effectively reduce NRL and increase cone-like photoreceptors in WT mice, a laser-induced CNV model, and an RP model using $Rho^{P23H/+}$ transgenic mice. Moreover, increased photoreceptor survival was demonstrated in $Rho^{P23H/+}$ mice treated with intravitreal cp-asiNRL. These results suggest the potential utility of cp-asiNRL as a new treatment strategy for retinal degenerative diseases.

Data availability

The raw and processed scRNA-seq data used in this study have been deposited in GEO under accession number GSE266377 (https://www.ncbi.nlm.nih.gov/geo/query/acc.cgi?acc=GSE266377, secure token: ydknumoqvryhdgt). All other data that support the findings of this study are available from the corresponding author Hyewon Chung (hchung@kuh.ac.kr) upon reasonable request.

Received: 21 January 2025; Accepted: 13 June 2025
Published online: 26 July 2025

References

1. Rim, T. H., Park, H. W., Kim, D. W. & Chung, E. J. Four-year nationwide incidence of retinitis pigmentosa in South Korea: a population-based retrospective study from 2011 to 2014. *BMJ Open.* **7**, e015531. https://doi.org/10.1136/bmjopen-2016-015531 (2017).
2. Li, J. Q. et al. Prevalence and incidence of age-related macular degeneration in Europe: a systematic review and meta-analysis. *Br. J. Ophthalmol.* **104**, 1077–1084 (2020).
3. Teo, C. L. et al. Prevalence of retinitis pigmentosa in singapore: the Singapore Epidemiology of Eye Diseases Study. *Acta Ophthalmol.* **99**, e134–e135. https://doi.org/10.1111/aos.14483 (2021).
4. de Cabral, T. A., Daich Varela, M., Georgiou, M. & Michaelides, M. Treatments for dry age-related macular degeneration: therapeutic avenues, clinical trials and future directions. *Br. J. Ophthalmol.* **318452** https://doi.org/10.1136/bjophthalmol-2020-318452 (2021).
5. Schaffrath, K. et al. One-Year safety and performance assessment of the Argus II retinal prosthesis: a postapproval study. *JAMA Ophthalmol.* **137**, 896–902 (2019).
6. Maguire, A. M. et al. Efficacy, safety, and durability of voretigene neparvovec-rzyl in RPE65 mutation–associated inherited retinal dystrophy: results of phase 1 and 3 trials. *Ophthalmology* **126**, 1273–1285 (2019).
7. Sahel, J. A. et al. Partial recovery of visual function in a blind patient after optogenetic therapy. *Nat. Med.* **27**, 1223–1229. https://doi.org/10.1038/s41591-021-01351-4 (2021).
8. Gasparini, S. J., Llonch, S., Borsch, O. & Ader, M. Transplantation of photoreceptors into the degenerative retina: current state and future perspectives. *Prog. Retin. Eye Res.* **69**, 1–37 (2019).
9. Ribeiro, J. et al. Restoration of visual function in advanced disease after transplantation of purified human pluripotent stem cell-derived cone photoreceptors. *Cell. Rep.* **35**, 109022 (2021).
10. Zerti, D. et al. Transplanted pluripotent stem cell-derived photoreceptor precursors elicit conventional and unusual light responses in mice with advanced retinal degeneration. *Stem Cells* (2021).
11. Singh, M. S. et al. Transplanted photoreceptor precursors transfer proteins to host photoreceptors by a mechanism of cytoplasmic fusion. *Nat. Commun.* **7**, 1–5 (2016).
12. Mandai, M. et al. iPSC-derived retina transplants improve vision in rd1 end-stage retinal-degeneration mice. *Stem Cell. Rep.* **8**, 69–83 (2017).
13. Lux, A., Llacer, H., Heussen, F. M. & Joussen, A. M. Non-responders to bevacizumab (Avastin) therapy of choroidal neovascular lesions. *Br. J. Ophthalmol.* **91**, 1318–1322. https://doi.org/10.1136/bjo.2006.113902 (2007).
14. Sadda, S. R., Guymer, R., Monés, J. M., Tufail, A. & Jaffe, G. J. Anti–vascular endothelial growth factor use and atrophy in neovascular age-related macular degeneration: systematic literature review and expert opinion. *Ophthalmology* **127**, 648–659 (2020).
15. Rezvani, M. et al. In vivo hepatic reprogramming of myofibroblasts with AAV vectors as a therapeutic strategy for liver fibrosis. *Cell. Stem Cell.* **18**, 809–816 (2016).
16. Song, G. et al. Direct reprogramming of hepatic myofibroblasts into hepatocytes in vivo attenuates liver fibrosis. *Cell. Stem Cell.* **18**, 797–808 (2016).
17. Wang, H., Yang, Y., Liu, J. & Qian, L. Direct cell reprogramming: approaches, mechanisms and progress. *Nat Rev. Mol. Cell. Biol* **2021**, 1–15 (2021).
18. Davis, R. L., Weintraub, H. & Lassar, A. B. Expression of a single transfected cDNA converts fibroblasts to myoblasts. *Cell* **51**, 987–1000 (1987).
19. Ieda, M. et al. Direct reprogramming of fibroblasts into functional cardiomyocytes by defined factors. *Cell* **142**, 375–386 (2010).
20. Vierbuchen, T. et al. Direct conversion of fibroblasts to functional neurons by defined factors. *Nature* **463**, 1035–1041 (2010).
21. Jorstad, N. L. et al. Stimulation of functional neuronal regeneration from Müller glia in adult mice. *Nature* **548**, 103–107. https://doi.org/10.1038/nature23283 (2017).
22. Yao, K. et al. Restoration of vision after de Novo genesis of rod photoreceptors in mammalian retinas. *Nature* **560**, 484–488. https://doi.org/10.1038/s41586-018-0425-3 (2018).
23. Mears, A. J. et al. Nrl is required for rod photoreceptor development. *Nat. Genet.* **29**, 447–452. https://doi.org/10.1038/ng774 (2001).
24. Montana, C. L. et al. Reprogramming of adult rod photoreceptors prevents retinal degeneration. *Proc. Natl. Acad. Sci. U.S.A.* **110**, 1732–1737. https://doi.org/10.1073/pnas.1214387110 (2013).
25. Yu, W. et al. Nrl knockdown by AAV-delivered CRISPR/Cas9 prevents retinal degeneration in mice. *Nat. Commun.* **8**, 14716. https://doi.org/10.1038/ncomms14716 (2017).
26. Crudele, J. M. & Chamberlain, J. S. Cas9 immunity creates challenges for CRISPR gene editing therapies. *Nat. Commun.* **9**, 3497. https://doi.org/10.1038/s41467-018-05843-9 (2018).
27. Alkan, F., Wenzel, A., Anthon, C., Havgaard, J. H. & Gorodkin, J. CRISPR-Cas9 off-targeting assessment with nucleic acid duplex energy parameters. *Genome Biol.* **19**, 177–177. https://doi.org/10.1186/s13059-018-1534-x (2018).
28. Reich, S. J. et al. Small interfering RNA (siRNA) targeting VEGF effectively inhibits ocular neovascularization in a mouse model. *Mol. Vis.* **9**, 210–216 (2003).
29. Shen, J. et al. Suppression of ocular neovascularization with SiRNA targeting VEGF receptor 1. *Gene Ther.* **13**, 225–234. https://doi.org/10.1038/sj.gt.3302641 (2006).
30. Kaur, H. et al. Diabetes-induced extracellular matrix protein expression is mediated by transcription coactivator p300. *Diabetes* **55**, 3104–3111 (2006).
31. Natoli, R. et al. Retinal macrophages synthesize C3 and activate complement in AMD and in models of focal retinal degeneration. *Invest. Ophthalmol. Vis. Sci.* **58**, 2977–2990 (2017).

32. Chen, S. H. & Zhaori, G. Potential clinical applications of SiRNA technique: benefits and limitations. *Eur. J. Clin. Invest.* **41**, 221–232 (2011).
33. Watts, J. K. & Corey, D. R. Silencing disease genes in the laboratory and the clinic. *J. Pathol.* **226**, 365–379 (2012).
34. Hwang, J. et al. Development of cell-penetrating asymmetric interfering RNA targeting connective tissue growth factor. *J. Invest. Dermatology*. **136**, 2305–2313 (2016).
35. Chang, C. I. et al. Asymmetric shorter-duplex SiRNA structures trigger efficient gene Silencing with reduced nonspecific effects. *Mol. Ther.* **17**, 725–732 (2009).
36. Percie du Sert. The ARRIVE guidelines 2.0: updated guidelines for reporting animal research. *PLoS Biol.* **18**, e3000410. https://doi.org/10.1371/journal.pbio.3000410 (2020).
37. Lambert, V. et al. Laser-induced choroidal neovascularization model to study age-related macular degeneration in mice. *Nat. Protoc.* **8**, 2197–2211. https://doi.org/10.1038/nprot.2013.135 (2013).
38. Lee, J. et al. Angiopoietin-1 suppresses choroidal neovascularization and vascular leakage. *Invest. Ophthalmol. Vis. Sci.* **55**, 2191–2199. https://doi.org/10.1167/iovs.14-13897 (2014).
39. Sakami, S. et al. Probing mechanisms of photoreceptor degeneration in a new mouse model of the common form of autosomal dominant retinitis pigmentosa due to P23H Opsin mutations. *J. Biol. Chem.* **286**, 10551–10567. https://doi.org/10.1074/jbc.M110.209759 (2011).
40. Chiang, W. C. et al. Robust endoplasmic reticulum-associated degradation of rhodopsin precedes retinal degeneration. *Mol. Neurobiol.* **52**, 679–695. https://doi.org/10.1007/s12035-014-8881-8 (2015).
41. Menon, M. et al. Single-cell transcriptomic atlas of the human retina identifies cell types associated with age-related macular degeneration. *Nat. Commun.* **10**, 4902. https://doi.org/10.1038/s41467-019-12780-8 (2019).
42. Bumcrot, D., Manoharan, M., Koteliansky, V. & Sah, D. W. RNAi therapeutics: a potential new class of pharmaceutical drugs. *Nat. Chem. Biol.* **2**, 711–719 (2006).
43. Corey, D. R. Chemical modification: the key to clinical application of RNA interference? *J. Clin. Invest.* **117**, 3615–3622 (2007).
44. Nykänen, A., Haley, B. & Zamore, P. D. ATP requirements and small interfering RNA structure in the RNA interference pathway. *Cell* **107**, 309–321 (2001).
45. Orozco, L. D. et al. Integration of eQTL and a single-cell atlas in the human eye identifies causal genes for age-related macular degeneration. *Cell Rep.* **30**, 1246–1259 e1246. https://doi.org/10.1016/j.celrep.2019.12.082 (2020).
46. Hu, Y. et al. Dissecting the transcriptome landscape of the human fetal neural retina and retinal pigment epithelium by single-cell RNA-seq analysis. *PLoS Biol.* **17**, e3000365. https://doi.org/10.1371/journal.pbio.3000365 (2019).
47. Voigt, A. P. et al. Single-cell transcriptomics of the human retinal pigment epithelium and choroid in health and macular degeneration. *Proc. Natl. Acad. Sci. U.S.A.* **116**, 24100–24107. https://doi.org/10.1073/pnas.1914143116 (2019).
48. Wolfrum, C. et al. Mechanisms and optimization of in vivo delivery of lipophilic siRNAs. *Nat. Biotechnol.* **25**, 1149–1157 (2007).
49. Ge, Q. et al. Effects of chemical modification on the potency, serum stability, and immunostimulatory properties of short ShRNAs. *RNA* **16**, 118–130 (2010).
50. Jo, S. et al. Selection and optimization of asymmetric SiRNA targeting the human c-MET gene. *Mol. Cells.* **32**, 543–548 (2011).
51. Hong, S. W. et al. Effect of the guide strand 3′-end structure on the gene-silencing potency of asymmetric SiRNA. *Biochem. J.* **461**, 427–434 (2014).
52. Curcio, C., Millican, C. L., Allen, K. & Kalina, R. Aging of the human photoreceptor mosaic: evidence for selective vulnerability of rods in central retina. *Invest. Ophthalmol. Vis. Sci.* **34**, 3278–3296 (1993).
53. Ronquillo, C. C. et al. Ciliopathy-associated IQCB1/NPHP5 protein is required for mouse photoreceptor outer segment formation. *FASEB J.* **30**, 3400 (2016).
54. Haider, N. B., Naggert, J. & Nishina, P. M. Excess cone cell proliferation due to lack of a functional NR2E3 causes retinal dysplasia and degeneration in rd7/rd7 mice. *Hum. Mol. Genet.* **10** (16), 1619–1626 (2001).

Author contributions

H.L. and H.J. have full access to all the data in the study and take full responsibility for the integrity of the data and the accuracy of the data analyses. Conceptualization and design were conducted by H.C. and D.K.L., while methodology development was led by H.L., H.J., J.C., H.K.L., and C.P. Software development was performed by H.K.L. and S.L. Validation was carried out by H.L., H.J., D.K.L., and H.C., and formal analysis was conducted by H.J. The investigation was performed by H.L., H.J., J.C., H.K.L., C.S., C.P., T.H., M.Y., S.P., S.W.H., S.Y.L., and J.L. Resources were provided by H.C., and data curation was completed by H.J. and J.C. The original draft was prepared by H.L. and H.J., with D.K.L. and H.C. contributing to the review and editing. Visualization was handled by H.L., C.S., and H.J., while supervision, project administration, and funding acquisition were managed by H.C. H.L. and H.J. contributed equally to this study. All authors critically reviewed and approved the final manuscript.

Funding

This study was supported by the National Research Foundation of Korea, funded by the Ministry of Science and ICT (grant numbers RS-2019-NR037345, RS-2020-NR046274 and RS-2024-00453840).

Competing interests

H.J., T.H., M.Y., S.P., S.W.H., and D.K.L. are employees of OliX Pharmaceuticals Inc. H.C. serves as a consultant for OliX Pharmaceuticals Inc. A related patent application has been filed: PCT/KR2021/018460. The remaining authors - H.L., J.C., H.K.L., C.S., C.P., S.Y.L., J.L., and S.L. - declare no competing interests.

Additional information

Supplementary Information The online version contains supplementary material available at https://doi.org/10.1038/s41598-025-07299-6.

Correspondence and requests for materials should be addressed to D.K.L. or H.C.